MATERIALS OF ELECTRONICS

UDC 538.911: 538.975 DOI: 10.15222/TKEA2017.6.34

*A. F. BELYANIN[1], V. V. BORISOV[2], S. A. DAGHETSYAN[3], S. A. EVLASHIN[2], A. A. PILEVSKY[2], V. A. SAMORODOV[2]*

Russia, Moscow, [1]Central Research Technological Institute "Technomash", [2]Skobeltsyn Institute of Nuclear Physics, [3]Lomonosov Moscow State University
E-mail: belyanin@cnititm.ru

# CARBON NANOWALLS IN FIELD EMISSION CATHODES

*The carbon nanowall (CNW) layers were grown from a gas mixture of hydrogen and methane, activated by a DC glow discharge, on Si substrates (Si/CNW layered structure). The second layer of CNW was grown either on the first layer (Si/CNW/CNW structure) or on Ni or NiO films deposited on the first CNW layer (Si/CNW/Ni/CNW and Si/CNW/NiO/CNW structures). The composition and structure of the resulting layered structures were studied using scanning electron microscopy, Raman spectroscopy, and X-ray diffractometry. It was found that annealing of Si/CNW structure in vacuum, growing of the second CNW layer on Si/CNW, as well as deposition of Ni or NiO films prior to the growing of the second CNW layer improve functional properties of field emission cathodes based on the electron-emitting CNW layers.*

*Keywords: carbon nanowalls, layered structures, electron microscopy, Raman spectroscopy, field emission cathodes.*

Carbon materials, including various crystalline (diamond, graphite) and noncrystalline (fullerene, nanotubes, graphene, etc.) ordered substances with unique physicochemical properties are of practical interest. Some carbon materials due to the autoemission property are promising for use as an emitting layer of field emission cathodes (autocathodes). The presence of field emission means a decrease in the electric field strength to 1–10 V/μm, which is required for the onset of field emission of electrons. Autocathodes are used in the development of X-ray tubes, microwave devices, electron guns for exciting lasers, cathodoluminescent lighting devices, flat displays and other devices [1–5]. The most promising for the creation of autocathodes with a low electron emission barrier are the so-called carbon nanowalls **(CNW)** — layers of a plate-like carbon material with a predominant orientation of the plates perpendicular to the substrate [1–3].

The layers of carbon materials formed by plasma methods, including CNW, are as a rule multiphase layers [6–8]. The structure and concentration of crystalline and X-ray amorphous phases depend on the conditions for carbon materials formation and affect their emission properties. The problems of using CNW in autocathodes are associated with the instability of emission parameters (magnitude and density of the cathode current, as well as the degree of electrical current uniformity over the cathode area) due to changes in composition and structure during testing and operation [4, 6, 8].

Before being placed into electrovacuum devices and soldered, autocathodes are always preliminaryly tested in a vacuum chamber for compatibility with the parametres of the device. In some cases, preliminary tests are carried out to achieve such required parameters as autoemission current and its stability in time. Stability tests can be performed both in the voltage stabilization mode [4] and in the current stabilization mode. In the first case we consider cathode current dependence (decrease) on time at a fixed stabilized voltage, in the second case — voltage dependence (growth) on time at a fixed stabilized current. In both cases, the graphs of the dependencies (hereinafter aging curves) objectively characterize the degradation (aging) of the autocathode, regardless of what causes it.

Storing the tested autocathodes with CNW layers on open air also leads to a deterioration of their emission properties. This is caused by the fact that during vacuum testing on the surface of CNW plates, the layer of adsorbed hydrocarbons is destroyed. This layer normally prevents adsorption of the components of the air mixture (water and nitrogen molecules, etc.) that impair the emission characteristics of the autocathodes [4, 15]. To recover the emission properties of autocathodes that had passed preliminary tests, they are annealing in vacuum or in an inert gas

atmosphere at a temperature of about 720 K [6]. Autocathodes that had not passed preliminary tests (even without vacuum breakdown), as a rule are not further used.

We can assume that autocathodes with a second CNW layer should have better emission properties than autocathodes with only the first CNW layer annealed. Moreover, for autocathodes that had not been preliminaryly tested, growing of the second CNW layer on top of the first one should increase the yield ratio for vacuum electronics.

This study researches how vacuum annealing and growing of a second CNW layer affects the emission properties of layered autocathodes based on carbon nanostructures.

### Samples used in the research

The CNW samples were grown on Si substrates from a gas mixture of hydrogen ($H_2$) and methane ($CH_4$) activated by a DC glow discharge [3, 6]. Before growing CNW, priming carbon centers were created on the substrate. For this purpose, at a temperature of 1020 K, the surface of the substrate was bombarded with $H^+$ and $C_xH_y^+$ ions (high frequency discharge, 13.56 MHz, 40 W, 20 min), formed in the microwave plasma mixture of hydrogen and methane (8 – 10 volume % $CH_4$) at pressure of $6{,}6 \cdot 10^3$ Pa. Silicon substrates with seed particles were treated in $H_2$ plasma, after which a CNW layer was grown at a substrate temperature of 800 – 1300 K and a deposition rate of 6 μm/h. Emission characteristics of the obtained Si/CNW layered structures were tested for 0.5 hour.

Si/CNW structures that were tested and/or stored in the open air for a long time (1 to 3 years) were either annealed in vacuum, or a second CNW layer was grown on their surface under the same conditions as the first layer. In a vacuum ($10^{-3}$ – $10^{-5}$ Pa), the samples were annealed for 1.5 hours at 720 K (Si/CNW(ann) structure). When the second layer was grown, the crystallites of the first layer acted as seed centers of the second layer. The second layer of CNW was also grown on the surface of the first layer of CNW coated with Ni or NiO.

Ni films were obtained by magnetron sputtering from a Ni target with a direct current in an argon atmosphere (Si/CNW/Ni structure). The conditions for obtaining Ni films are as follows: Ar pressure 1.2 – 1.5 Pa; discharge power 900 W; substrate temperature 420 – 570 K; deposition rate 1.5 μm/h. The thickness $h$ of the resulting Ni films was 10, 40, 80, and 160 nm (Si/CNW/Ni$^h$ structures).

NiO films were formed in two stages. At the first stage, a 0.25% solution of $Ni(NO_3)_2$ was applied to the CNW layer in a 50% hydroalcoholic ($H_2O$ + $C_2H_5OH$) mixture at room temperature, followed by heat treatment at 420 K. The heat treatment caused the crystalline hydrate $Ni(NO_3)_2 \cdot 6H_2O$ formed during heat treatment to decompose to NiO form at a temperature of 370 – 410 K.

$Ni(NO_3)_2$ was deposited at atmospheric pressure either by immersing the substrate with a CNW layer in a solution, followed by heat treatment (the result was the Si/CNW/NiO structure) or by aerosol precipitation (5 – 10 cycles of 1 minute with heat treatment after each cycle, the result was the Si/CNW/NiO* structure). To generate the aerosol, the Albedo IN-8 (Альбедо ИН-8) halogenator was used with an average mass median aerodynamic diameter of the aerosol particles of 3.94 μm.

### Research technique

The CNW composition and the layered structures were studied using a Carl Zeiss Supra 40-30-87 scanning electron microscope (SEM), a Rigaku D/MAX-2500/PC X-ray diffractometer (Cu$k$ radiation) and a LabRAM HR800 (HORIBA Jobin-Yvon) laser Raman scattering spectrometer (632.8 nm line of He-Ne laser, beam spot diameter 4 μm$^2$, depth of the analyzed layer 3 μm).

Current-voltage (**I-V**) characteristics and aging curves that determine the dependence of voltage on time during long-term emission tests at a given current in the regime of constant current stabilization were obtained using a Pw2500_v2_3kV_1a source of stabilized pulsed current produced by SINP MSU and a Spellmann Sl30 source of stabilized direct current. The measurements were carried out in diode cells at a pressure of $5 \cdot 10^{-5}$ Pa.

To correctly compare the structures with the second layer of CNW, each sample with the first CNW layer was divided into two parts ($A$, $B$) equal in area which were used to co-grow a second layer of CNW in one charge. Part $A$ was used as control, and part $B$ was covered with a Ni or NiO layer, then the $A$:Si/CNW/CNW and $B$:Si/CNW/Ni/CNW (or $B$:Si/CNW/NiO/CNW) structures were compared. In the tests with annealing, the second CNW layer was not grown onto part $B$, while the first CNW layer was annealed, then the $A$:Si/CNW/CNW and $B$:Si/CNW(ann) structures were compared.

The I-V characteristic and the autoemission parameters of the samples were recorded in the pulsed mode of electric current measurement. The aging curves and their parameters were measured in the constant stabilized current mode.

Field emission tests were carried out on samples with a surface having intrinsic conductivity.

During measuring the I-V characteristic in the pulsed mode, a glass plate with a conductive layer of mixed indium-tin oxide (ITO, chemical formula: $(In_2O_3)_{0.9}$-$(SnO_2)_{0.1}$) was used as an anode. The plate was covered with a luminophore layer. This anode completely covered the emitting surface of the sample. When measuring the aging curves in the constant stabilized current mode (10 mA), a water-cooled thick-walled (5 mm) copper anode was used with a polished working surface in the form of a 5×2×2 mm strip located above the 4×2 mm rectangular area of the autocathode.

The gap (Δ) between the surface of the autocathode and the anode was 250 μm when measured in pulsed mode and 125 μm — in direct current mode. The I-V characteristics were plotted in the coordinates ($E$, $J$), where $E = U/\Delta$ is the electric field strength in the gap between the anode and the autocathode, $J = I/S$ is the current density, $U$ is the potential difference between the electrodes; $I$ is the current of the autocathode, $S$ is the working area of the autocathode. According to the I-V characteristics, Fowler—Nordheim diagrams were plotted in ($E^{-1}$, $\ln(J/E^2)$) coordinates.

### Composition and structure of CNW

Carbon nanowalls are a porous material formed by curved lamellar (scaly) clusters of X-ray amorphous and crystalline phases of carbon (**Fig. 1**).

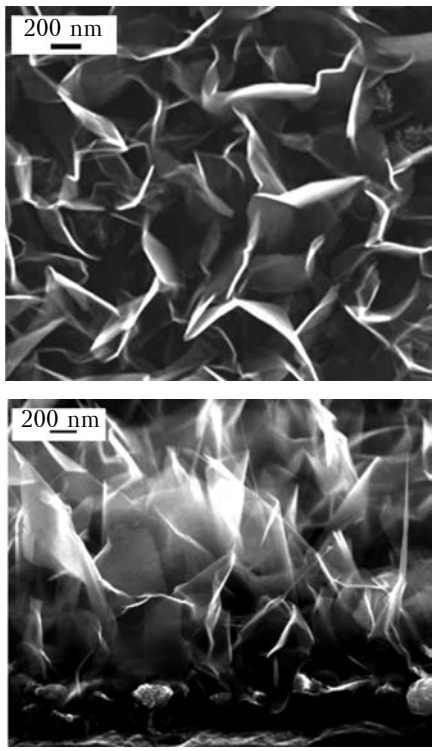


Fig. 1. SEM image of the Si/CNW layer structure: *a* — CNW growth surface; *b* — Si/CNW cleavage

The CNW plates were 3—10 nm thick [3]. Apart from bent carbon plates, the structure of CNW samples also contain rods (plates folded into tubes), nanotubes and equiaxed particles with an average size of 40—50 nm (Fig. 1, *b*).

X-ray diffractometry shows that CNW contains mainly graphite ($P6_3/mmc$ spatial group) and carbyne (hexagonal syngony), as well as phases of diamond ($Fd\bar{3}m$), chaotite ($P6/mmm$ spatial group) and graphite modifications ($R3$ and $P3$ spatial groups) [6, 8]. The thickness of the CNW plates corresponds to the size of the crystallites (X-ray coherent scattering regions, $L_{CSR}$) equal to 8.5—9.5 nm and calculated from the broadening on X-rays of diffraction peaks of 0002 graphite.

In the Raman spectra of the Si/CNW layer structure, which explicitly reflect the composition and structure of CNW [9, 10], we can observe intense *D, G* and 2*D* bands, located at the Raman shift Δν, equal to 1330—1343, 1577—1591 and 2660—2673 $cm^{-1}$, respectively. At the same time, weak bands are fixed at Δν equal to 233—243, 863—879 and 1081—1167 $cm^{-1}$ (*x* band); 1612—1627 (*D*' band); 2449—2482 (*x*+*D* band); 2909—2934 (*D*+*G* band) and 3221—3248 $cm^{-1}$ (2*D*' band). (In this study we denote CNW Raman spectral bands as *D*, *G*, *x*, *D*', *x*+*D*, 2*D*, *D*+*G* и 2*D*' [11—13].)

**Fig. 2** (curve *1*) shows the Raman spectrum of one of the Si/CNW samples. The values of the intensity ratio of the main CNW Raman spectral bands depending on their formation conditions have a considerable spread: $I_D/I_G = 0.32—2.03$; $I_D/I_{2D} = 0.98—1.23$; $I_D/I_{D+G} = 14.1—17.6$; $I_D/I_{2D} = 13.0—16.1$ [6, 8].

The CNW Raman spectra were compared with similar spectra of highly oriented pyrolytic UPV-1T (УПВ-1Т) graphite (Fig. 2, curve *2*). The 2*D* graphite band consists of two components: $2D_1$ and $2D_2$ (Fig. 2, curves *3, 4*) with an intensity proportional to the one of the *G* band. In contrast to the 2*D* graphite band, the 2*D* CNW band is symmetrical, which is characteristic of graphene [9, 13]. The differences in the 2*D* band in the CNW and graphite Raman spectra are caused by a significant curvature of individual regions of the graphite atomic layers {0001}, which disrupts atomic bonds inside and between the layers.

Depending on the degree of the CNW plates curvature (curvature radius 590—770 nm), the 2*D* band changes shape, which reflects changes in the electronic bands corresponding to the positions of atoms in the lattice. The layers in such a crystallite (CNW plates) form a hexagonal lattice (two-layer stacking of carbon atoms) [1, 6, 14]. If we consider the CNW crystallites as graphite plates, then their size (plate thickness) calculated

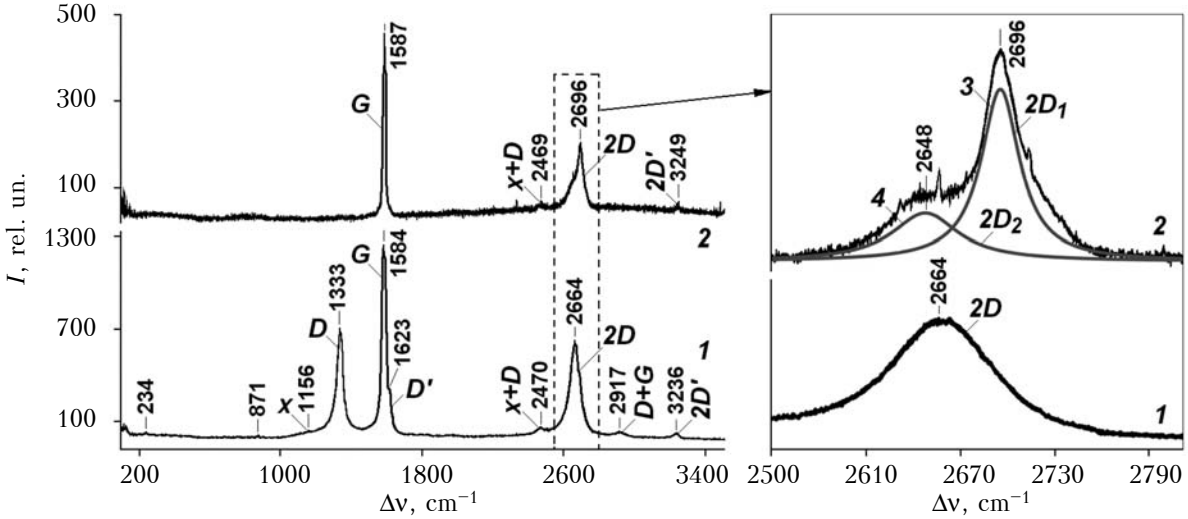


Fig. 2. Raman spectra of Si/CNW (*1*) and graphite (*2*) layered structures. Inset graph shows a fragment of the spectra in the Δν range of 2550–2800 $cm^{-1}$ (*3* and *4* are Lorentz distribution functions, which in sum approximate curve *2*)

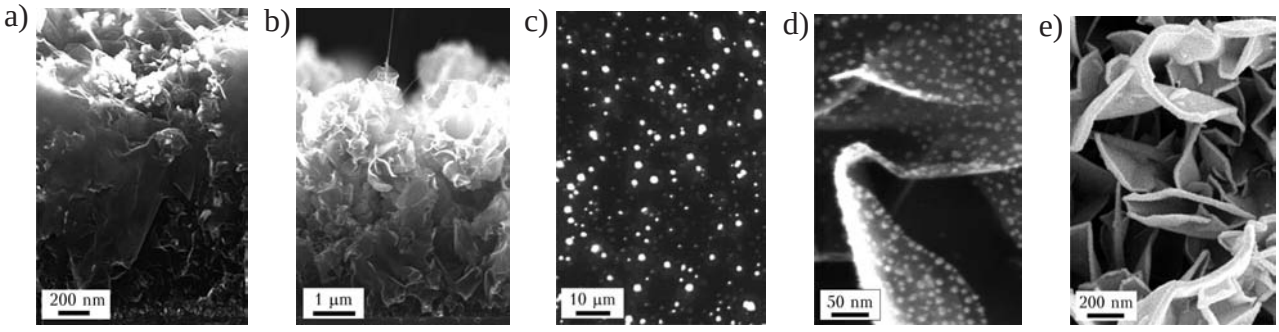


Fig. 3. SEM images of the samples:
*a* – Si/CNW (cleavage); *b* – Si/CNW/NiO*/CNW (cleavage); *c* – Si/CNW/NiO*; *d* – Si/CNW/$Ni^{10}$; *e* – Si/CNW/$Ni^{80}$

from the intensitiy ratio of the *D* and *G* ($I_D/I_G$) Raman spectral bands would be $L = 3.3–9.9$ nm. The obtained size is close to the values calculated from the X-rays. Taking into account that the interplanar distance of graphite (0001 plane) is 0.335 nm, one can state that there are about 10–30 layers of graphene in a CNW plate.

The maximum height of the first CNW layer starting from the substrate is 2–4 μm, the total height of the first and second layers is approximately 8.5 μm (**Fig. 3**, *a*, *b*). After the heat treatment of the Si/CNW layered structure covered with $Ni(NO_3)_2\ 6H_2O$ crystal hydrate, NiO crystallites less than 2 μm in size were formed on the surface of the CNW (Fig. 3, *c*). The deposition of a 10 nm thick Ni film on the CNW layer (Si/CNW/$Ni^{10}$ structure) by magnetron sputtering resulted in the formation of an islet structure with a cluster size less than 10 nm (Fig. 3, *d*). A continuous $Ni^h$ film (thickness $h > 40$ nm) was formed mainly on the CNW edges located at a 90° angle to the Ni particles flux during magnetron sputtering (Fig. 3, *d*). On all other CNW surfaces, the Ni film thickness was by orders of magnitude smaller.

**Fig. 4**, *a, b* shows the globular structure of the CNW layers with a globule diameter of 1.5–2 μm. The second layer of CNW, deposited on a NiO film, has a more dense packing of globules and a larger thickness of the plates (Fig. 4, *d*). Samples *A*:Si/CNW/CNW and *B*:Si/CNW/$Ni^{10}$/CNW (Fig. 4, *a, b*) contain a large number of nanotubes with a diameter of 10–40 nm, while in samples with Ni or NiO films their number does not exceed 1–2 per globule.

The structure of the second CNW layer is characterized by the presence of carbon plates on the crystallites (plates) of the first layer, including multiwall nanotubes (Fig. 4, *c*). In the Si/CNW/$Ni^{160}$/CNW and Si/CNW/NiO*/CNW samples, thickened crystallites of carbon plates with rounded edges (not typical) were found (Fig. 4, *d*, *e*). It was discovered that on average

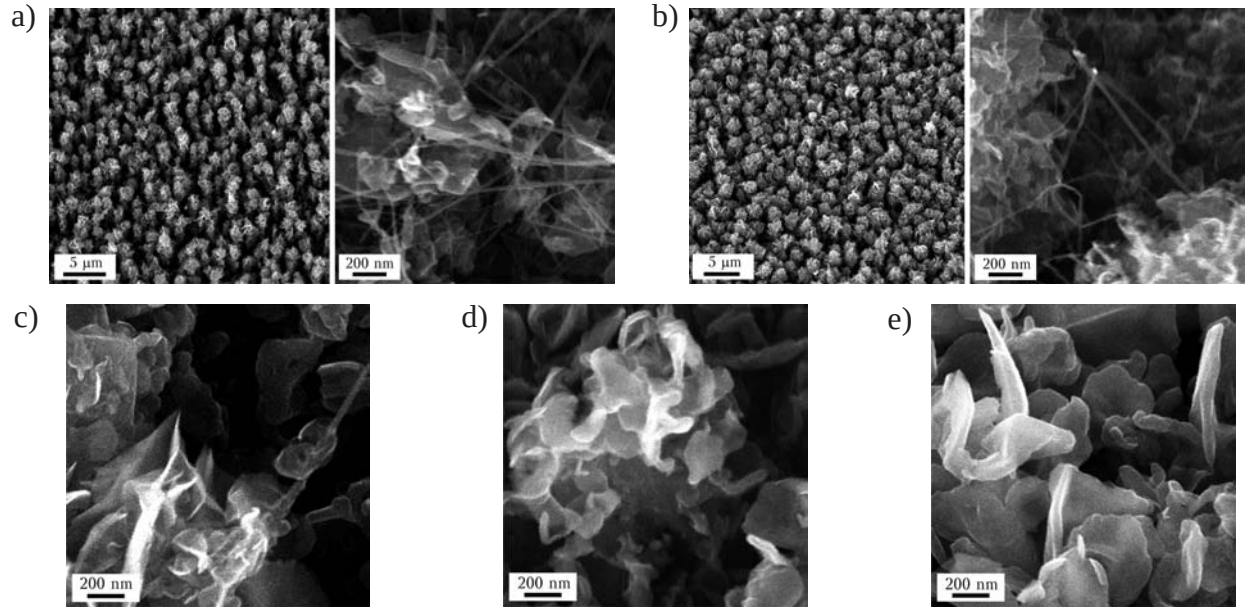


Fig. 4. SEM images of surfaces of layered structures:
*a* — $A_1$:Si/CNW/CNW; *b* — $B_1$:Si/CNW/Ni$^{10}$/CNW;
*c* — $B_2$:Si/CNW/Ni$^{10}$/CNW; *d* — Si/CNW/Ni$^{160}$/CNW; *e* — Si/CNW/NiO*/CNW
(right-hand images in *a* and *b* are scaled-up fragments of the surface of the second CNW layer)

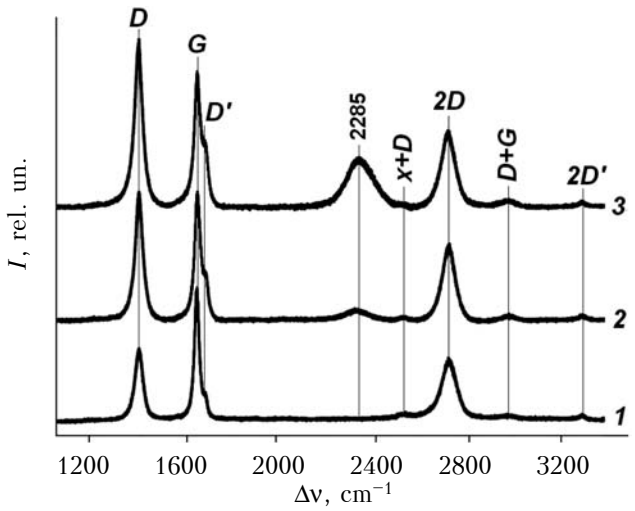


Fig. 5. CNW Raman spectra before and after growing the second CNW layer:
*1* — *A*:Si/CNW; *2* — *A*:Si/CNW/CNW;
*3* — *B*:Si/CNW/NiO*/CNW

the maximum height of the second CNW layer was 2.4 times greater than that of the first; the globular structure of the second CNW layer became more dense and homogeneous; the number of multiwall nanotubes decreased; on the Raman spectrum of the second CNW layer with a globular structure, a band appeared at $\Delta\nu = 2285$ cm$^{-1}$ **(Fig. 5, Table 1)**.

The Raman spectra shown in Fig. 5 are normalized to the intensity of the 2*D* ($I_{2D}$) band. On the Raman spectra of the Si/CNW/NiO*/CNW structure, the band intensity at $\Delta\nu = 2285$ cm$^{-1}$ increased almost 4-fold. The wide band at $\Delta\nu = 2262-2286$ cm$^{-1}$ (broadening of the $\Delta\nu_{1/2} = 120-160$ cm$^{-1}$ band) was manifested in the Raman spectra of CNW after annealing at temperatures above 870 K [7]. A similar band was also observed on the Raman spectra of polycluster diamond films produced by the microwave discharge method [3].

The crystallite size ($L_{CSR}$), the number of graphene layers ($N$), and the $I_{2D}/I_D$ parameter

Table 1

*Structural parameters of the upper layer of CNW layered structures*

| Layered structure | $\Delta\nu_{1/2}$, cm$^{-1}$ | $I_D$ | $I_G$ | $I_{D'}$ | $I_{2D}$ | $I_D/I_G$ | $L_{CSR}$ | $N$ | $I_{D'}/I_G$ | $I_{2D}/I_D$ | $I_{2D}/I_G$ | $I_{2285}$ |
|---|---|---|---|---|---|---|---|---|---|---|---|---|
| Si/CNW | 19.4 | 228.3 | 388.8 | 113.4 | 202 | 0.6 | 7.5 | 22 | 0.3 | 0.9 | 0.5 | 0 |
| Si/CNW/CNW | 17.7 | 340.6 | 338.1 | 130.5 | 202 | 1.0 | 4.4 | 13 | 0.4 | 0.6 | 0.6 | 337 |
| Si/CNW/NiO*/CNW | 19.9 | 442.4 | 356.9 | 176.5 | 202 | 1.2 | 3.6 | 10 | 0.5 | 0.5 | 0.6 | 130.2 |

of the samples *A*:Si/CNW; *A*:Si/CNW/CNW and *B*:Si/CNW/NiO*/CNW (in this order) decreased, while the $I_{D'}/I_G$, $I_{2D}/I_G$ parameters and $I_{2285}$ band intensity increased (Table 1).

### Emission properties of CNW-based autocathodes

Simultaneously with the I-V measurement, a sequence of images was registered on an luminophore anode screen. Obviously, in this sequence, you should select an image with the worst visual uniformity, which is located in the middle part of the sequence, while at its beginning and at its end there are images that are visually evaluated as homogeneous: almost black ones, obtained at small electric fields, at the beginning, and lighted ones, obtained at large electric fields, at the end **(Fig. 6)**.

To assess the uniformity of images, subjective (visual) criteria are often used. Of the many objective homogeneity criteria based on digital image processing, we chose the simplest criterion based on variation coefficient. We used the intensity (brightness) of a pixel in a gray raster image as the random variable. Uniformity of the image (in percent) was calculated from a sample consisting of all pixels of the image, according to the formula

$$H = 100V - 33,$$

where $V$ is variation coefficient, $V = \sigma / \overline{X}$; $\sigma$ and $\overline{X}$ are the mean square deviation and average linear deviation in the sample, respectively.

In statistical data processing, the sample is considered homogeneous if $V \le 0.33$ ($H \le 0\%$). For the sequence of images obtained from the luminophore anode screen, maximum of $H$ (the worst homogeneity) was taken as homogeneity $H^{\Delta}$. As can be seen from Fig. 6, the visual estimation of homogeneity coincides with the maximum at $H^{250} = -16.8\%$. The $H^{\Delta}$ parameter can be regarded as an estimate of the homogeneity of the cathode current distribution in the working region of the authocathode at the $\Delta$ gap.

It is known [4, 15] that the electric field around a pointed conductor is amplified and can be represented as $\beta E_0$, where $\beta$ is the field gain near a single emitter and approximately equals to the aspect ratio (height/transverse dimension) of the conductor; $E_0$ is the ideal electric field strength equal to $U/\Delta$. Assuming that all emission centers have regular geometry (the same sizes and relative position), the dependencies on the Fowler–Nordheim **(FN)** diagrams are described by the equation of the straight line $y = Bx + C$, where $x = 1/E$, $y = \ln(J/E^2)$. The slope ratio of the straight line $B$ is a value proportional to $\beta$, while the density of the emissive centers $D_E$ is proportional to the $\exp(C)$ value ($C$ is the segment cut off by the straight line on the ordinate axis).

For the given films, a linear region can be distinguished on the curves of the FN diagrams [17]. For a relative comparison of the values characterizing emission properties of the autocathodes, it is sufficient to assume that in this linear region only emission centers with regular geometry generate the electrical current, while the contribution of the others to the resulting current is negligible [4, 15]. As emission characteristics of the autocathodes, we considered the following: the autoemission threshold, $E_T$, is the minimum value of $E$ at which the emission current is registered; the estimation of the aspect number of a single emitter in the regular geometry $\beta$; the estimation of density of emission centers in the regular geometry $D_E$; homogeneity $H^{250}$ in a sequence of emission images.

The aging curves **(AC)** for the structures with the second CNW layer were obtained as the voltage $U$ on time $T$ dependence at a constant current of 10 mA, measured in the current stabilization mode. The 10 mA value of current was chosen due to the capabilities of the equipment available, as well as to current density limitations ($J \approx 0.12$ mA/cm$^2$), at which undesirable vacuum breakdowns are unlikely in the test cell. The aging curves allowed determining the aging rate for 6 hours ($V_{6h}$), for 3 hours ($V_{3h}$) and for the last hour ($V_{1h}$) of tests. A comparison of the aging curves of $A$ and $B$ parts of samples with a second CNW layer was carried out using the $Q_{AB}$ parameter that takes into account the relative position of these curves

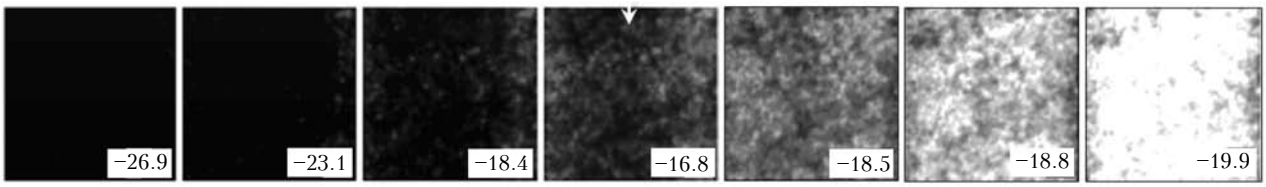


Fig. 6. Sequence of 2×2 mm emission images with different homogeneity $H^{250}$ (the values in % are given in the images)

along the ordinate ($U$) and the ratio of the areas bounded by these curves and the abscissa axis:

$$Q_{AB} = (S_A/(S_A+S_B)) - 0.5,$$

where $S_B$ is the area under the $AC_B$ for $B$:Si/CNW/Ni$^h$/CNW, $B$:Si/CNW/NiO/CNW, $B$:Si/CNW(ann);

$S_A$ is the area under the $AC_A$ of the corresponding $B$ control structures $A$:Si/CNW/CNW (or $A$:Si/CNW in the case of annealing).

If the $AC_B$ is located above the $AC_A$, then $-0.5 < Q_{AB} < 0$ (part $B$ has a higher voltage); if $AC_B$ is located below $AC_A$, then $0.5 > Q_{AB} > 0$ (part $B$ is less high-voltage). The smaller $|Q_{AB}|$, the closer are the $AC_A$ and $AC_B$ areas. At the same time, the $|Q_{AB}| < 0.5$ inequality is valid.

**Fig. 7** presents the I-V characteristic curves and the FN lines described above for the parts of a single sample of layered structure, and their parameters are given in **Table 2**. As can be seen from the presented data, the parts without the second CNW layer ($A$:Si/CNW и $B$:Si/CNW) are characterized by a high autoemission threshold ($E_T \geq 5.6$ V/μm), a large aspect ratio β (which confirms the presence of a large number of multiwall nanotubes on the first CNW layer), a low density of emission centers $D_E$, and a low homogeneity of field emission images ($H^{250} \geq 0$).

Parts with a second CNW layer (structures $B$:Si/CNW/CNW/NiO*/CNW and $A$:Si/CNW/CNW) are characterized by a lower autoemission threshold ($E_T \leq 3.6$ V/μm), a smaller value of β, a higher $D_E$ density, as well as a better images uniformity ($H^{250} \leq 0$). For a given sample, the part with the $A$:Si/CNW/CNW structure is characterized by better values of the parameters $E_T$, β, $H^{250}$, $V_{3h}$, $V_{1h}$ than the $B$:Si/CNW/NiO*/CNW structure, and the values of the $D_E$ parameter for them are virtually identical.

Examples of the arrangement of the I-V characteristics and the aging curves of the samples with the Si/CNW/NiO*/CNW (sample 1) and Si/CNW(ann) (sample 2) structures are shown in **Fig. 8, 9**.

As can be seen from Fig. 8, for sample 1, the I-V characteristic of the $B_1$:Si/CNW/NiO*/CNW

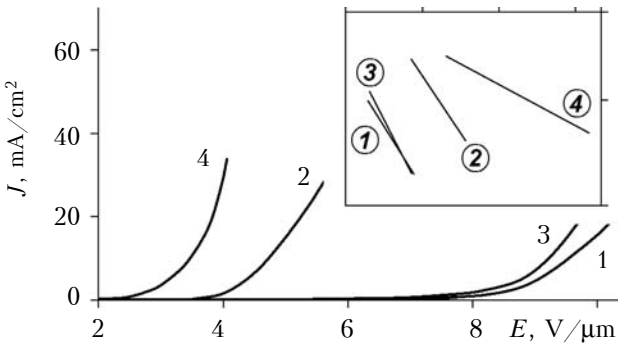


Fig. 7. Example of the I-V characteristics and their linear representations in the FN coordinates (see inset) obtained for the following layered structures:

*1* — $A$:Si/CNW; 2 — $B$:Si/CNW/NiO*/CNW; *3* — $B$:Si/CNW; *4* — $A$:Si/CNW/CNW

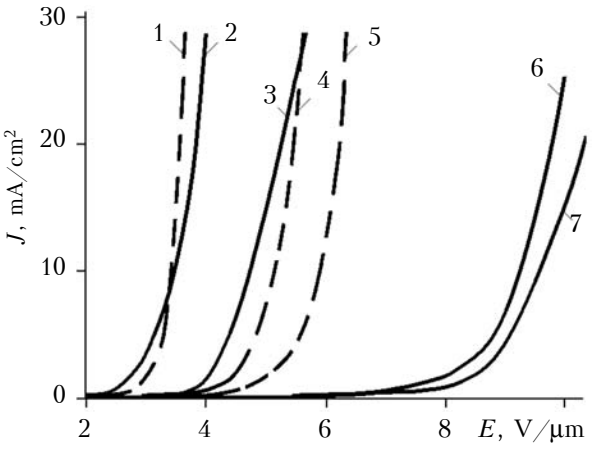


Fig. 8. I-V characteristics of layered structures of two samples:

Sample 1 (solid lines): *2* — $B_1$:Si/CNW/NiO*/CNW; *3* — $A_1$:Si/CNW/CNW; *6* — $A_1$:Si/CNW; *7* — $B_1$:Si/CNW; Sample 2 (dashed lines): *1* — $A_2$:Si/CNW/CNW; *4* — $B_2$:Si/CNW(ann); *5* — $A_2$:Si/CNW

Table 2

*Example of emission characteristics of autocathode parts on layered structures*

| Structure | Measuring mode | | | | | | | |
|---|---|---|---|---|---|---|---|---|
| | Pulse | | | | Continuous | | | |
| | $E_T$, V/μm | β | ln($D_E$) | $H^{250}$, % | $V_{6h}$, V/h | $V_{3h}$, V/h | $V_{1h}$, V/h | $Q_{AB}$ |
| $A$:Si/CNW | 6.1 | 42.7 | 1.9 | 39.07 | — | — | — | — |
| $B$:Si/CNW/NiO*/CNW | 3.6 | 32.9 | 6.0 | −10.52 | 50 | 33 | 10 | 0.18 |
| $B$:Si/CNW | 5.6 | 47.0 | 3.0 | 29.36 | — | — | — | — |
| $A$:Si/CNW/CNW | 2.4 | 21.1 | 5.9 | −7.18 | 10 | 0 | 0 | — |

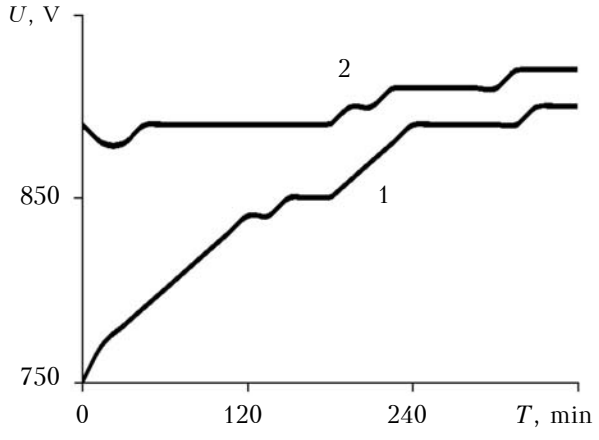


Fig. 9. Aging curves of layered structures of sample 1 for 6 hour tests:
*1* — $B_1$:Si/CNW/NiO*/CNW; *2* — $A_1$:Si/CNW/CNW

structure (curve *2*) is shifted to the left by 4 V/μm relative to the I-V characteristics of the $A_1$:Si/CNW and $B_1$:Si/CNW structures (curves *6, 7*) and by 1.5 V/μm relative to the I-V characteristic for the $A_1$:Si/CNW/CNW (curve *3*).

For sample 2, the I-V characteristic of the $B_2$:Si/CNW(ann) structure (curve *4*) is shifted to the left by 0.8 V/μm relative to the I-V characteristic of the $A_2$:Si/CNW (curve *5*) and to the right by 1.8 V/μm relative to the I-V characteristic of the $A_2$:Si/CNW/CNW (curve *1*). This indicates that the emission properties of the autocathode with a second CNW layer deposited on the NiO* oxide layer have improved in comparison with the autocathode with the second CNW layer without the oxide, as well as that the emission properties of the autocathode with the second CNW layer have improved in comparison with an autocathode that had only undergone a restorative annealing of the first CNW layer.

According to the data from Table 2 and Fig. 9, for $B_1$:Si/CNW/NiO*/CNW and $A_1$:Si/CNW/CNW structures, the $Q_{AB}$ parameter is 0.1 for 6 hours of testing, 0.18 for 3 hours and 0.08 for the last hour. In this case, the $AC_B$ for $B_1$:Si/CNW/NiO*/CNW turns out to be less high-voltage than the $AC_A$ for $A_1$:Si/CNW/CNW, but it loses to the $AC_A$ in the aging rate. The behavior of the $AC_A$ and $AC_B$ during 6 hour tests ($Q_{AB}$ = 0.1) shows their asymptotic convergence at positive values of $Q_{AB}$, which can be explained by the fact that the second CNW layer on the $A_1$ and $B_1$ parts was grown simultaneously during the same charge.

A summary data of the averaged characteristics of the investigated autocathodes is presented in **Table 3**. The averaging was carried out according to the groups (samples) of the parts of the layered structures indicated in the table. The sample sizes corresponded to the number of parts in each of the groups.

The analysis of the data from Table 3 shows the following. Regardless of which film is used

Table 3

*Mean values (M) and standard deviations (S) of the emission characteristics of parts of autocathodes on layered structures*

| Structure | Sample size | | Measurement mode | | | | | | |
|---|---|---|---|---|---|---|---|---|---|
| | | | Pulse | | | Continuous | | | |
| | | | $E_{T,}$ V/μm | β | ln($D_E$) | $H^{250}$, % | $V_{3h}$, V/h | $V_{1h}$, V/h | $Q_{AB}$ |
| *A*:Si/CNW; *B*:Si/CNW | 26 | M | 4.5 | 60.6 | 7.2 | 11.8 | — | — | — |
| | | S | 1.3 | 24.7 | 2.5 | 19.9 | — | — | — |
| *A*:Si/CNW/CNW | 13 | M | 2.3 | 37.5 | 9.2 | −2.5 | 20.0 | 10.8 | — |
| | | *S* | 1.1 | 20.5 | 3.0 | 17.7 | 21.3 | 13,2 | — |
| *B*:Si/CNW (ann) | 3 | M | 3.1 | 53.3 | 10.2 | −14.2 | 11.1 | 13.3 | −0.01 |
| | | S | 0.1 | 9.1 | 1.4 | 10.8 | 10.2 | 15.3 | 0.41 |
| *B*:Si/CNW/NiO/CNW | 2 | M | 3.5 | 58.2 | 13.0 | −6.0 | 5.0 | 15.0 | 0.44 |
| | | S | 0.3 | 4.3 | 0.9 | 3.6 | 21.2 | 21.2 | 0.06 |
| *B*:Si/CNW/NiO*/CNW | 2 | M | 2.6 | 33.6 | 8.5 | 2.1 | 16.7 | 10.0 | 0.32 |
| | | S | 1.3 | 1.0 | 1.7 | 17.8 | 23.6 | 0 | 0.19 |
| *B*:Si/CNW/$Ni^{10}$/CNW | 3 | M | 1.9 | 34.1 | 10.0 | −16.4 | 14,4 | 3.3 | 0.14 |
| | | S | 0.3 | 11.4 | 1.7 | 2.8 | 5.1 | 5.8 | 0.32 |
| *B*:Si/CNW/$Ni^{40}$/CNW | 1 | M | 2.2 | 36.5 | 6.8 | −2.9 | 26.7 | 0 | −0.48 |
| *B*:Si/CNW/$Ni^{80}$/CNW | 1 | M | 2.9 | 35.4 | 7.4 | −7.3 | 20.0 | 10.0 | −0.50 |
| *B*:Si/ CNW/$Ni^{160}$/CNW | 1 | M | 3.2 | 53.4 | 13.1 | −3.8 | 13.3 | 0 | −0.12 |

(Ni or NiO), the presence of the second CNW layer reduces the average value of the $E_T$ emission threshold to about 2.3 V/μm as compared to the average value of 4.5 V/μm for the first CNW layer. The average $E_T$ values for the second CNW layer structures with or without Ni, NiO film differ by approximately 0.1%. On average, the best results for the $E_T$ parameter (1.9 V/μm) were shown by the Si/CNW/Ni$^{10}$/CNW structures, for which the aging rate is also minimal ($V_{1h} \approx 3.3$ V/h) with a positive $Q_{AB}$ value of 0.14. The best $V_{1h}$ results had the Si/CNW/Ni$^{40}$/CNW and Si/CNW/Ni$^{160}$/CNW structures ($V_{1h} = 0$) at low $E_T$ values, however for these structures the $Q_{AB}$ parameter turned out to be negative.

Because of the large number of multiwall nanotubes [16], the autocathodes without both the second CNW layer and restorative annealing of the first CNW layer showed the best results for the β parameter (60.5 on average) with a low density of emission centers ($D_E \approx 10^3$, $\ln(D_E) = 7.2$). Then the β parameter was decreasing in structures with a second layer in the following order: Si/CNW/NiO/CNW and Si/CNW/Ni$^{160}$/CNW. These same structures with the minimum number of multiwall nanotubes showed the best result for the $D_E$ parameter ($D_E \approx 10^5$, $\ln(D_E) = 13$).

As to the homogeneity of the emission images, the best results on the average were shown by the Si/CNW/Ni$^{10}$/CNW structures ($H^{250} = -16.4\%$). Then the $H^{250}$ parameter was getting worse (increasing) in structures in the following order: Si/CNW(ann), Si/CNW/Ni$^{80}$/CNW, Si/CNWNiO/CNW, Si/CNW/Ni$^{160}$/CNW, Si/CNW/Ni$^{40}$/CNW, Si/CNW/NiO$^*$/CNW, and finally the worst were Si/CNW structures.

## Conclusion

Thus, the analysis of the I-V characteristics and aging curves of autocathodes based on Si/CNW, Si/CNW/CNW, Si/CNW/Ni/CNW and Si/CNW/NiO/CNW layered structures, as well as the assessment of homogeneity of the images obtained on the luminiferous anode screen allowed establishing the following. On average, the emission properties of autocathodes with a second CNW layer and the presence (optional) of a Ni or NiO film between the CNW layers are better than those of autocathodes that undergo restorative vacuum annealing of the first layer at 720 K. Of all the tested autocathodes with a second layer, the best results on the emission characteristics were shown by the autocathodes with 10 nm thick islet Ni films, which indicates the possibility to use similar cathodes in vacuum electronics. However, for better statistical validity, it is necessary to collect a larger amount of experimental data.

REFERENCES

1. Tzeng Y., Chen C-L., Chen Y-Y., Liu C-Y. Carbon nanowalls on graphite for cold cathode applications. *Diamond and Related Materials*, 2010, vol. 19 (2-3), pp. 201-204.

2. Wang H-X., Jiang N., Zhang H., Hiraki A. Growth of a three dimensional complex carbon nanoneedle electron emitter for fabrication of field emission devices. *Carbon*, 2010, vol. 48, pp. 4483-4488. https://doi.org/10.1016/j.diamond.2009.08.005

3. Belyanin A.F., Borisov V.V., Bagdasarian A.S. *Rossiiskii tekhnologicheskii zhurnal*, 2017, vol. 5, no. 3, pp. 22-40. (Rus)

4. Egorov N., Sheshin E. Field emission electronics. *Springer Series in Advanced Microelectronics*, 2017, vol. 60, pp. 568, http://dx.doi.org/10.1007/978-3-319-56561-3

5. Busta H.H., Chen J.M., Shen Z., Jansen K., Rizkowski S., Matey J., Lanzillotto A. Characterization of electron emitters for miniature X-ray sources. *Journal of Vacuum Science & Technology B*, 2003, vol. 21, pp. 344–349. https://doi.org/10.1007/978-3-319-56561-3

6. Belyanin A.F., Borisov V.V., Samoylovich M.I., Bagdasarian A.S. On the effect of laser irradiation and heat treatment on the structure and field-emission properties of carbon nanowalls. *Journal of Surface Investigation: X-ray, Synchrotron and Neutron Techniques*, 2017, vol. 11, no. 2, pp. 295-304. http://dx.doi.org/10.1134/S1027451017020057]

7. Belyanin A.F., Borisov V.V., Nalimov S.A., Bagdasarian A.S. *Nanomaterials and nanostructures - XXI century*, 2017, vol. 8, no. 3, pp. 34–42. (Rus)

8. Belyanin A.F., Samoylovich M.I., Borisov V.V., Evlashin S.A. [Study of multiphase carbon films of field emission cathodes electron microscopy, raman spectroscopy and X-ray diffraction method]. *Nano- and Microsystems Technology*, 2014, no. 2, pp. 20-25. (Rus)

9. Ferrari A.C. Raman spectroscopy of graphene and graphite: Disorder, electron-phonon coupling, doping and nanodiabatic effects. *Solid State Communications*, 2007, vol. 143, pp. 47-57. https://doi.org/10.1016/j.ssc.2007.03.052

10. Pimenta M.A., Dresselhaus G., Dresselhaus M.S., Cancado L.G., Jorio A., Saito R. Studying disorder in graphite-based systems by Raman spectroscopy. *Physical Chemistry Chemical Physics*, 2007, vol. 9, pp. 1276-1291. http://dx.doi.org/10.1039/B613962K

11. Ferrari A.C., Meyer J.C., Scardaci V., Casiraghi C., Lazzeri M., Mauri F., Piscanec S., Jiang D., Novoselov K.S., Roth S., Geim A.K. Raman spectrum of graphene and graphene layers. *Physical Review Letters*, 2006, vol. 97, 187401. https://doi.org/10.1103/PhysRevLett.97.187401

12. Shang N.G., Staedler T., Jiang X. Radial textured carbon nano flake spherules. *Applied Physics Letters*, 2006, 89, 103112. https://doi.org/10.1063/1.2346314

13. Jackson Di Martino Thornton. *Carbon Nanowalls: Processing, Structure and Electrochemical Properties.* A dissertation submitted to the Graduate Faculty of North Carolina State University, 2011, 55 p.

14. Tzeng Y, Chen W. L, Wu C., Lo J-Y., Li C-Y. The synthesis of graphene nanowalls on a diamond film on a silicon substrate by direct-current plasma chemical vapor deposition. *Carbon*, 2013, vol. 53, pp. 120-129. https://doi.org/10.1016/j.carbon.2012.10.038

15. Eletskii A. V. Carbon nanotube-based electron field emitters. 2010 *Phys.-Usp.* 53 863. https://doi.org/10.3367/UFNe.0180.201009a.0897

16. Borisov V.V., Pilevskii A.A., Samorodov V.A. *Nanomaterials and nanostructures - XXI century*, 2017, vol. 8, no. 2, pp. 37-41. (Rus)

17. Smol'nikova E.A. *Investigation of the structural and autoemission characteristics of nanografic cold cathodes.* A dissertation submitted to the Graduate, 2015, Lomonosov Moscow State University, 146 p. (Rus)

*Received 21.11 2017*

DOI: 10.15222/TKEA2017.6.34
УДК 538.911: 538.975

*А. Ф. БЄЛЯНІН[1], В. В. БОРИСОВ[2], С. А. ДАГЕСЯН[3], С. А. ЄВЛАШИН[2], А. А. ПІЛЕВСЬКИЙ[2], В. А. САМОРОДОВ[2]*

Росія, м. Москва, [1]ЦНДТІ «Техномаш», [2]НДІ ядерної фізики ім. Д. В. Скобельцина МДУ;
[3]Московський державний університет ім. М. В. Ломоносова
E-mail: belyanin@cnititm.ru

# ВУГЛЕЦЕВІ НАНОСТІНКИ В АВТОЕМІСІЙНИХ КАТОДАХ

*Вуглецеві матеріали, що включають різні кристалічні (алмаз, графіт) і некристалічні (фуллерен, нанотрубки, графен та ін.) впорядковані речовини з унікальними фізико-хімічними властивостями, представляють практичний інтерес. Деякі вуглецеві матеріали завдяки властивості автоемісії є перспективними для використання як емітуючого шару автоемісійних катодів (автокатодів). Найбільш перспективними для створення автокатодів з низьким бар'єром емісії електронів вважаються так звані вуглецеві наностінкі ($C_H$) — шари пластинчастого вуглецевого матеріалу з переважним орієнтуванням пластин перпендикулярно підкладці. Роботу присвячено дослідженню впливу відпалу в вакуумі і нарощеного другого шару $C_H$ на емісійні властивості шаруватих автокатодів на основі вуглецевих наностінок.*

*Шари $C_H$ для досліджень вирощували з газової суміші $H_2$ і $CH_4$, активованої тліючим розрядом постійного струму, на підкладках з Si. Перед нарощуванням $C_H$ на підкладках створювалися вуглецеві затравочні центри шляхом обробки поверхні іонами $H^+$ та $C_xH_y^+$. Емісійні характеристики отриманих шаруватих структур $Si/C_H$ контролювали півгодинними випробуваннями. Піддані випробуванням та/або тривалому зберіганню на відкритому повітрі шаруваті структури $Si/C_H$ або відпалювали в вакуумі (1,5 години при 720 К), або на їх поверхні нарощували другий шар $C_H$ ($Si/C_H/C_H$) за тих же умов, що і перший. Другий шар $C_H$ нарощували також на поверхні першого шару $C_H$, вкритого плівкою Ni або NiO (структури $Si/C_H/Ni/CH$ та $Si/C_H/NiO/C_H$). Плівки Ni отримували методом магнетронного розпилення, а плівки NiO — термічною обробкою в розчині $Ni(NO_3)_2$. Максимальна висота першого шару $C_H$ щодо підкладки становила 2—4 мкм, сумарна висота першого і другого шарів — 8,5 мкм. Склад і будову шаруватих структур досліджували з використанням растрової електронної мікроскопії, рентгенівської дифрактометрії і спектрометрії комбінаційного розсіювання світла.*

*Емісійні властивості представлено у вигляді статистичних оцінок порогу автоемісії, коефіцієнту посилення електричного поля поблизу одиночного автоемітера і щільності емісійних центрів в регулярній геометрії, однорідності емісійних зображень, а також швидкості старіння автоемісійних катодів за тривалих випробувань на постійному стабілізованому струмі. Розроблена методика випробувань дозволила проводити коректне порівняння емісійних характеристик автоемісійних катодів до і після вирощування другого шару $C_H$, а також після відпалу в вакуумі. Встановлено, що в середньому емісійні властивості автокатодів з другим шаром $C_H$ і плівкою Ni або NiO між шарами $C_H$ є кращими, ніж у автокатодів, які пройшли відновлювальний відпал у вакуумі першого шару за температури 720 К. Відзначено, що з усіх досліджених автокатодів з другим шаром $C_H$ найкращі результати за емісійними характеристиками в середньому показали автокатоди з острівковими плівками Ni товщиною 10 нм. Проведені дослідження підтверджують можливість застосування шаруватих автокатодів на основі вуглецевих наностінок в пристроях вакуумної електроніки.*

*Ключові слова: вуглецеві наностінки, шаруваті структури, електронна мікроскопія, спектроскопія комбінаційного розсіяння світла, автоемісійні катоди.*

---

*Д. т. н. А. Ф. БЕЛЯНИН[1], В. В. БОРИСОВ[2], С. А. ДАГЕСЯН[3], к. ф-м. н. С. А. ЕВЛАШИН[2], А. А. ПИЛЕВСКИЙ[2], В. А. САМОРОДОВ[2]*

Россия, г. Москва,[1]ЦНИТИ «Техномаш», [2]НИИ ядерной физики им. Д. В. Скобельцына,
[3]Московский государственный университет им. М. В. Ломоносова

E-mail: belyanin@cnititm.ru

# УГЛЕРОДНЫЕ НАНОСТЕНКИ В АВТОЭМИССИОННЫХ КАТОДАХ

*Слои углеродных наностенок ($C_H$) выращивали из газовой смеси водорода и метана, активированной тлеющим разрядом постоянного тока, на подложках из Si (слоистая структура $Si/C_H$). Второй слой $C_H$ выращивали на первом слое (структура $Si/C_H/C_H$) или на пленках Ni или NiO, осажденных на первом слое $C_H$ (структуры $Si/C_H/Ni/CH$ и $Si/C_H/NiO/C_H$). Методами растровой электронной микроскопии, спектроскопии комбинационного рассеяния света и рентгеновской дифрактометрии исследованы состав и строение полученных слоистых структур. Установлено, что отжиг в вакууме структуры $Si/C_H$, наращивание на $Si/C_H$ второго слоя $C_H$, а также нанесение пленок Ni или NiO перед наращиванием второго слоя $C_H$ приводят к улучшению функциональных свойств автоэмиссионных катодов на основе слоев $C_H$, эмитирующих электроны.*

*Ключевые слова: углеродные наностенки, слоистые структуры, электронная микроскопия, спектроскопия комбинационного рассеяния света, автоэмиссионные катоды.*